



Short communication

Electrochemical performances of $\text{LiFe}_{1-x}\text{Mn}_x\text{PO}_4$ with high Mn content

Bin Zhang, Xiaojian Wang, Hong Li, Xuejie Huang*

Institute of Physics, Chinese Academy of Sciences, Beijing 100190, China

ARTICLE INFO

Article history:

Received 19 August 2010

Received in revised form 10 October 2010

Accepted 18 October 2010

Available online 23 October 2010

Keywords:

Olivine

Solid solution

Mesoporous

Overpotential

Cathode

Lithium ion batteries

ABSTRACT

A series of $\text{LiFe}_{1-x}\text{Mn}_x\text{PO}_4/\text{C}$ materials with high Mn content ($0.7 \leq x \leq 0.9$) are synthesized by solid state reaction. The samples have mesoporous structure with an average pore size of 25 nm, particle size around 200–300 nm, crystalline size around 30 nm and specific areas around $50 \text{ m}^2 \text{ g}^{-1}$. Their electrochemical performances are studied and the reversible capacity and rate performance decrease with the increase of Mn content. The redox potential of the $\text{Fe}^{2+}/\text{Fe}^{3+}$ and $\text{Mn}^{2+}/\text{Mn}^{3+}$ redox couple also shift accordingly. The overpotential value of the $\text{Mn}^{2+}/\text{Mn}^{3+}$ redox couple (80 mV) is close to that of the $\text{Fe}^{2+}/\text{Fe}^{3+}$ couple (60 mV) in all three compositions and shows a maximum ($\sim 300 \text{ mV}$) in the regions of voltage transition.

© 2010 Elsevier B.V. All rights reserved.

1. Introduction

Since the pioneer work of Goodenough and coworkers [1,2], olivine-structured LiMPO_4 ($\text{M} = \text{Fe}, \text{Mn}$) has been studied intensively as cathode materials for lithium ion batteries because of their high stabilities. However, intrinsic low electronic conductivity ($\sigma_e \sim 10^{-9} \text{ S cm}^{-1}$ for LiFePO_4 and $\sigma_e < 10^{-10} \text{ S cm}^{-1}$ at 300 K for LiMnPO_4) [3–5] and poor ionic transport property ($D_{\text{Li}} < 10^{-14} \text{ cm}^2 \text{ s}^{-1}$) [5,6] are the limiting factors for achieving high rate performances [7]. Decreasing the particle size [8–12] and applying carbon coating [13–18] are demonstrated as effective strategies for improving the kinetic properties of LiFePO_4 and LiMnPO_4 . However, electrochemical performances of LiMnPO_4 are still far from satisfaction. In consideration of high energy density and electrolyte compatibility, $\text{LiFe}_{1-x}\text{Mn}_x\text{PO}_4$ is of particular interest due to the relative high potential of $\text{Mn}^{2+}/\text{Mn}^{3+}$ redox couple at about 4.1 V vs Li/Li^+ , which can generate higher energy density especially with higher Mn content. Several researches have shown that the electrochemical activity of Mn in the solid solution of $\text{LiFe}_{1-x}\text{Mn}_x\text{PO}_4$ was significantly improved in the region $0 \leq x \leq 0.75$ [19–21]. For example, $\text{LiFe}_{0.4}\text{Mn}_{0.6}\text{PO}_4$ made by Yamada et al. and $\text{LiFe}_{0.25}\text{Mn}_{0.75}\text{PO}_4$ by Tohda et al. showed a capacity of 160 mAh g^{-1} and good cycling performances [19–21]. The simultaneous enhancement of electrochemical activity of Mn and Co in multi-component olivine materials such as $\text{LiFe}_{1/4}\text{Mn}_{1/4}\text{Co}_{1/4}\text{Ni}_{1/4}\text{PO}_4$ and $\text{LiFe}_{1/3}\text{Mn}_{1/3}\text{Co}_{1/3}\text{PO}_4$ are also

reported recently by some groups [22–24] with excellent electrochemical performances.

Previous investigations suggest that Mn-rich phase of $\text{LiFe}_{1-x}\text{Mn}_x\text{PO}_4$ ($x > 0.75$) is unsuitable for battery applications due to its poor kinetics and large lattice distortion of high Mn content [25]. However, it has been proved that nano-scale materials have advantages of enhanced transport kinetics and high reaction activity [26–28], in this paper, we have studied electrochemical performances of $\text{LiFe}_{1-x}\text{Mn}_x\text{PO}_4$ ($0.7 \leq x \leq 0.9$)/C with nanoporous structure. Meanwhile, thermodynamic and kinetic behaviors are also analyzed by a GITT (galvanostatic intermittent titration technique) [29] method to further understand the intrinsic properties of the high Mn content $\text{LiFe}_{1-x}\text{Mn}_x\text{PO}_4/\text{C}$ materials.

2. Experimental

Mesoporous $\text{LiFe}_{1-x}\text{Mn}_x\text{PO}_4/\text{C}$ was prepared by a solid state reaction. Stoichiometric amounts of Li_2CO_3 (Shanghai China Lithium, 99.9%), $\text{FeC}_2\text{O}_4 \cdot 2\text{H}_2\text{O}$ (Hefei Yalong 99%), $\text{MnC}_2\text{O}_4 \cdot 2\text{H}_2\text{O}$ (Hefei Yalong 99%), $\text{NH}_4\text{H}_2\text{PO}_4$ (Beijing Chemical 99.5%), appropriate quantity of citric acid (Beijing Chemical 99.5%) and sugar were mixed by using high energy ball milling with zirconia container for 5 h. The mixture was then sintered at 650°C for 10 h under argon atmosphere (99.9999%). Carbon contents of these samples were all about 18 wt% determined by Vario EL (Element, Germany). To confirm the chemical composition of these samples, the Fe/Mn ratios were determined by using ICP (IRIS Intrepid II) after complete dissolution of the powder into a hydrochloric acid solution. For these samples, the Li/Fe/Mn ratios are 1.02:0.29:0.69, 1.01:0.20:0.79 and 1.01:0.10:0.88 respectively, close to the target composition.

* Corresponding author. Tel.: +86 10 82648073; fax: +86 10 82649046.
E-mail address: xjhuang@aphy.iphy.ac.cn (X. Huang).

The structure was analyzed by a X-ray diffractometer (Rigaku Rint-2400) with Cu K α radiation at a scan rate of 0.02 (2θ) s^{-1} and the particle texture was observed by a scanning electron microscope (Hitachi S-4700) and a transmission electron microscope (TEM Philips CM12). Nitrogen adsorption/de-adsorption isotherm was performed at 77 K, in an Automatic Physorption and Chemsorption Analyzer (Micromeritics, Autosorb-1). Before the measurement, the sample was dried for 12 h at 623 K under the pressure of 10^{-3} Torr. The Brunauer–Emmett–Teller (BET) surface area (S_{BET}) was deduced from the isotherm analysis in the relative pressure (p/p^0) range of 0.04–0.20. The total pore volume (V_p) was calculated from the amount adsorbed at a relative pressure of 0.99. The average pore-size and pore size distribution were calculated according to the N $_2$ adsorption isotherm result using Barrett–Joiner–Halenda (BJH) method (column form pores).

The performances of the LiFe $_{1-x}$ Mn $_x$ PO $_4$ /C as cathode were evaluated using a Swagelock-type cell with lithium metal anode. The cathode was a mixture of LiFe $_{1-x}$ Mn $_x$ PO $_4$ /C, acetylene black and polyvinylidene fluoride (PVDF) with a weight ratio 75:10:15, and the electrolyte was a 1 M LiPF $_6$ -ethylene carbonate/dimethyl carbonate (EC/DMC) solution. The galvanostatic charge–discharge experiment was performed between 2.2 and 4.5 V on a Land automatic batteries tester (KINGNUO Electrical Co., Ltd, China) at room temperature. GITT was performed by charging/discharging the cell for 30 min at a constant current density of 17 mA g^{-1} (C/10) and relaxing for 12 h on an Arbin battery testing system.

3. Result and discussion

The XRD patterns of the mesoporous LiFe $_{1-x}$ Mn $_x$ PO $_4$ /C ($x=0.7, 0.8, 0.9$) samples show an orthorhombic structures ($Pnmb$) without any impurity (Fig. 1). Their crystallite size calculated by using the half peak width of XRD data by Sherrer equation [30] were estimated to be 31 nm, 30 nm, 37 nm. From the inset of Fig. 1, the position of the diffraction peaks shows a linear shift upon composition. It is due to the radius of Mn $^{2+}$ (0.83 nm) is slightly larger than that of Fe $^{2+}$ (0.78 nm). These materials have an average pore size of 25 nm with particle size ranging from 100 nm to 300 nm. LiFe $_{1-x}$ Mn $_x$ PO $_4$ /C ($x=0.7, 0.8, 0.9$) have specific surface areas of 49 m $^2 g^{-1}$, 57 m $^2 g^{-1}$, 53 m $^2 g^{-1}$, respectively. Using these samples with almost identical morphology and size, the electrochemical performances of the mesoporous LiFe $_{1-x}$ Mn $_x$ PO $_4$ /C ($x=0.7, 0.8, 0.9$) were investigated.

Fig. 2a shows the charge/discharge curves of these LiFe $_{1-x}$ Mn $_x$ PO $_4$ /C ($x=0.7, 0.8, 0.9$) samples at C/10. Discharge capacities are 130 mAh g^{-1} , 120 mAh g^{-1} and 110 mAh g^{-1} respectively. From the incremental capacity curves in Fig. 2b, it could

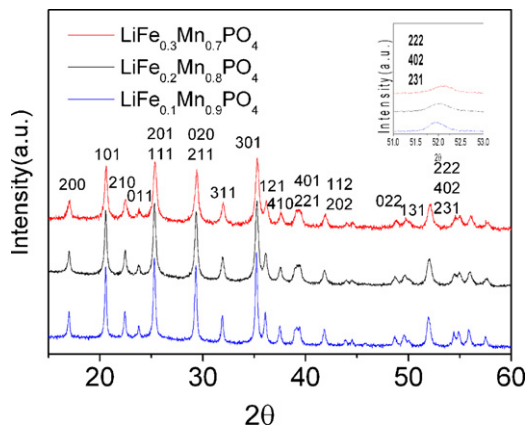


Fig. 1. XRD patterns of the mesoporous LiFe $_{1-x}$ Mn $_x$ PO $_4$ /C ($x=0.7, 0.8, 0.9$).

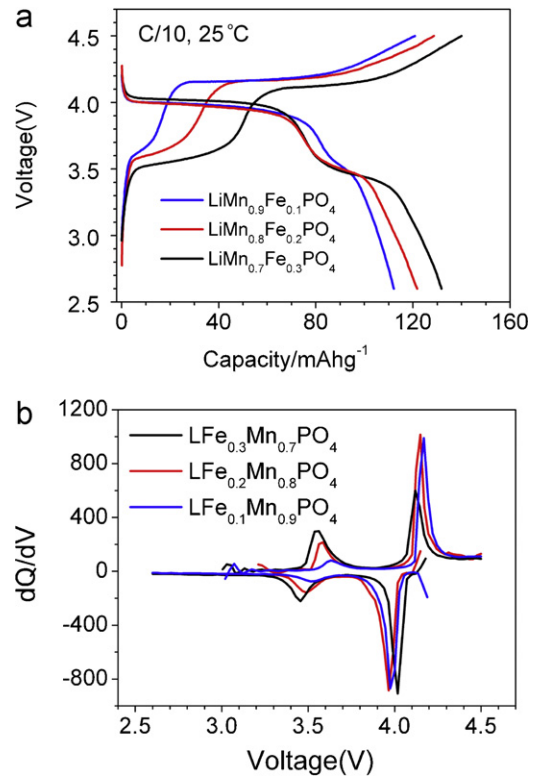


Fig. 2. Charge–discharge curves of the mesoporous LiFe $_{1-x}$ Mn $_x$ PO $_4$ /C ($x=0.7, 0.8, 0.9$). (a) galvanostatic curves at C/10, (b) incremental capacity curves.

be seen that LiFe $_{0.3}$ Mn $_{0.7}$ PO $_4$ /C has relatively smaller voltage hysteresis for Mn $^{2+}$ /Mn $^{3+}$ redox couple compared with that of LiFe $_{0.2}$ Mn $_{0.8}$ PO $_4$ /C and LiFe $_{0.1}$ Mn $_{0.9}$ PO $_4$ /C (detail value showed in Table 1). It showed also a relatively higher capacity. Voltage hysteresis of Mn $^{2+}$ /Mn $^{3+}$ redox couple increase with more Mn content, while that of Fe $^{2+}$ /Fe $^{3+}$ redox couple is not sensitive to the component. Table 1 also shows us the EMF values (electromotive force) estimated by the average potentials of the oxidation and reduction peaks. The EMF of Mn $^{2+}$ /Mn $^{3+}$ redox couple is almost unchanged in the three samples, while the EMF of Fe $^{2+}$ /Fe $^{3+}$ redox couple increases with increasing Mn content. Fig. 3 shows the cycle performances of the three LiFe $_{1-x}$ Mn $_x$ PO $_4$ /C ($x=0.7, 0.8, 0.9$) samples respectively. It is observed that the three samples have excellent cycle performances and the charge/discharge curves are almost unchanged up to 50 cycles. It is due to the stable olivine structure and the porous microstructure.

Fig. 4 shows the rate performances of the three LiFe $_{1-x}$ Mn $_x$ PO $_4$ /C ($x=0.7, 0.8, 0.9$) samples charging at C/10 then discharging from C/10 to 2C. At 2C rate, capacities of 90 mAh g^{-1} , 80 mAh g^{-1} and 70 mAh g^{-1} are achieved respectively. Rate performances of these materials are dependent on Fe/Mn ratio and they decrease with increasing Mn content. The origin of the composition dependent rate performances is presumably due to the low electronic and ionic conductivity of Mn rich olivine materials. Moreover, It could also be observed that the voltage hysteresis of Mn region is linear to the square of current density

Table 1
Voltage polarization of the LiFe $_{1-x}$ Mn $_x$ PO $_4$.

	LiFe $_{0.3}$ Mn $_{0.7}$ PO $_4$	LiFe $_{0.2}$ Mn $_{0.8}$ PO $_4$	LiFe $_{0.1}$ Mn $_{0.9}$ PO $_4$
ΔE (Mn $^{2+}$ /Mn $^{3+}$)	95 mV	140 mV	160 mV
ΔE (Fe $^{2+}$ /Fe $^{3+}$)	100 mV	95 mV	100 mV
EMF (Mn $^{2+}$ /Mn $^{3+}$)	4.065 V	4.05 V	4.06 V
EMF (Fe $^{2+}$ /Fe $^{3+}$)	3.5 V	3.52 V	3.57 V

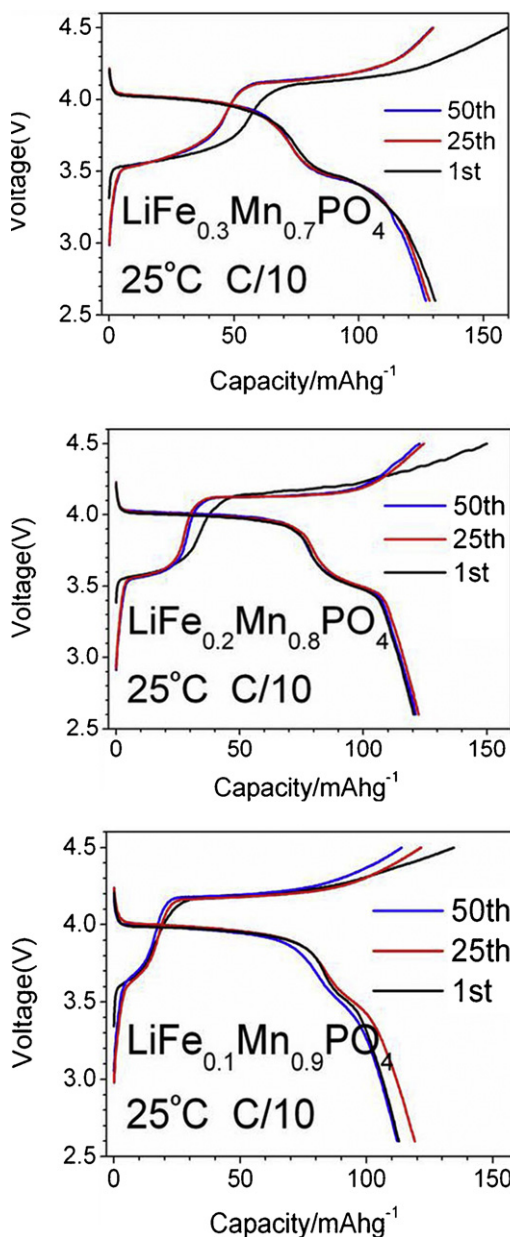


Fig. 3. Charge–discharge curves and cycle performances of the mesoporous $\text{LiFe}_{1-x}\text{Mn}_x\text{PO}_4/\text{C}$.

(Fig. 5a), which means that Li ion diffusion is the rate determining step. However, the voltage hysteresis of Mn region is not linear to log current (Fig. 5b), which means that the rate determining step is not the charge transfer process with a typical Tafel curve. Zero current overpotentials of the three samples obtained by extrapolating to zero current are equal to zero. This means the impedance resulting from charge transport is the only source of voltage hysteresis and there is no other thermodynamic origin in the electrochemical process [31].

GITT was performed further to study the thermodynamic and kinetic features of the materials. From GITT we could get the open circuit potential curves showed in Fig. 6. All the three samples show similar trend and a flat voltage profile in the $\text{Mn}^{2+}/\text{Mn}^{3+}$ region appears, which indicates a typical two phase reaction mechanism. A slope can be observed in the $\text{Fe}^{2+}/\text{Fe}^{3+}$ reaction region, which means a solid solution phase transformation mechanism. It is consistent with some recent work on multi-component olivine materials [22–25]. The dilution of transition metals in the olivine

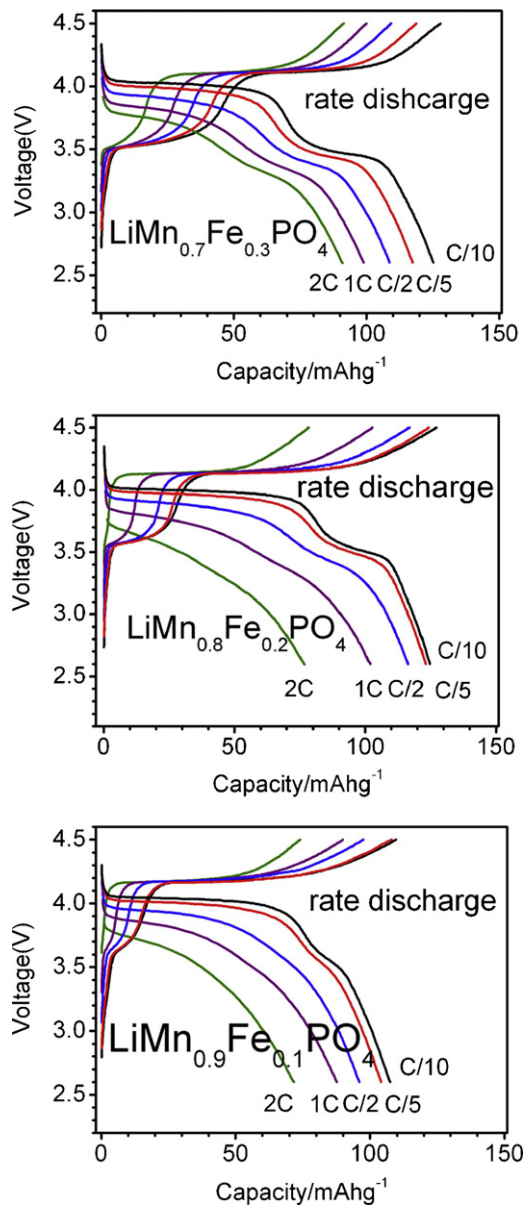


Fig. 4. Rate performances of the mesoporous $\text{LiFe}_{1-x}\text{Mn}_x\text{PO}_4/\text{C}$.

structure may have an internal effect upon binding energy and thus change the mechanism of electrochemical reaction. An intermediate reaction region can be seen clearly in between the $\text{Fe}^{2+}/\text{Fe}^{3+}$ slope region and $\text{Mn}^{2+}/\text{Mn}^{3+}$ plateau region.

From comparison of the open circuit voltages (OCVs) it could be observed that in the charging process the potential of $\text{Fe}^{2+}/\text{Fe}^{3+}$ redox couple increases obviously as Mn content increasing, while that of $\text{Mn}^{2+}/\text{Mn}^{3+}$ redox couple is almost constant at 4.08 V (Fig. 6a). The potential shift of $\text{Fe}^{2+}/\text{Fe}^{3+}$ redox couple with Mn content is related to the inductive effect of M–O bond [32] and the almost constant potential of $\text{Mn}^{2+}/\text{Mn}^{3+}$ redox couple should be attributed to the relatively small difference of Mn content among the samples. In the discharging process (Fig. 6b), OCVs showed a similar trend and could be explained accordingly.

The overpotentials can also be obtained from GITT method. Fig. 7 shows the overpotential profiles taken from the difference between the cut-off voltage and the open circuit voltage after 12 h relaxation. The three $\text{LiFe}_{1-x}\text{Mn}_x\text{PO}_4/\text{C}$ ($x=0.7, 0.8, 0.9$) samples show similar trend and has maximum overpotential appeared in the transformation regions from the $\text{Fe}^{2+}/\text{Fe}^{3+}$ redox couple to $\text{Mn}^{2+}/\text{Mn}^{3+}$ redox

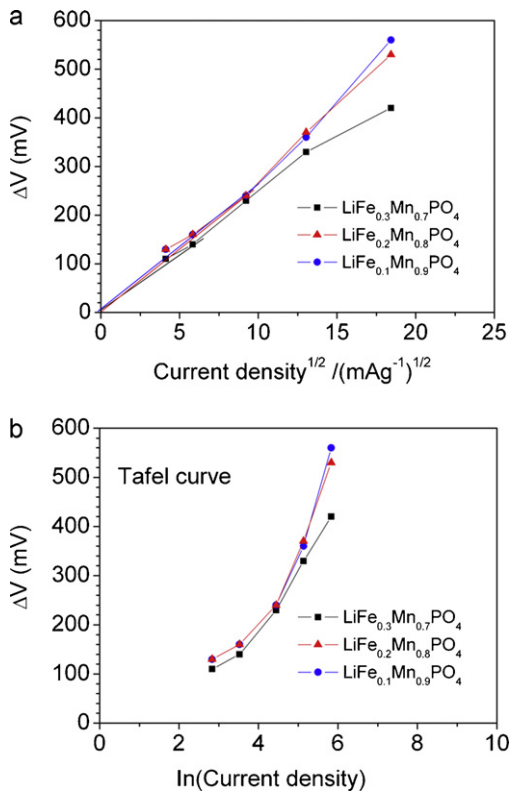


Fig. 5. Voltage hysteresis of Mn region vs different current density of the $\text{LiFe}_{1-x}\text{Mn}_x\text{PO}_4/\text{C}$.

couple. The phenomenon could be explained by presuming the transport of Li ion diffusion in the solid solution lattice is the rate determining step. During charging (lithium extraction), the first reaction regime corresponds to the single phase solid solution reaction for the Fe^{2+} oxidation. The diffusion length of Li ion is gradually increased from the surface to the core region of the particle, leading

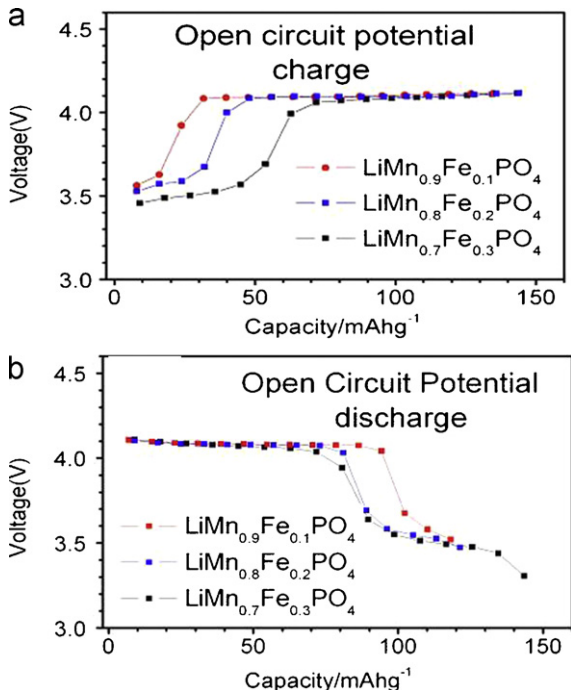


Fig. 6. Open circuit voltage curves of the $\text{LiFe}_{1-x}\text{Mn}_x\text{PO}_4/\text{C}$.

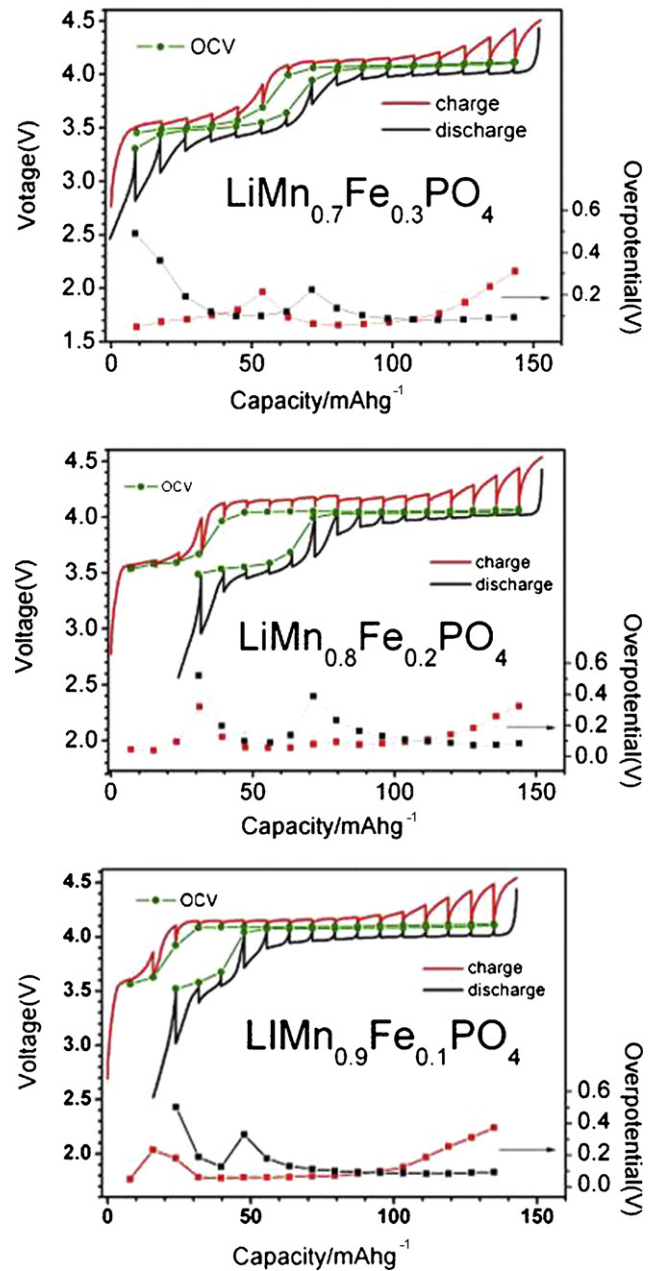


Fig. 7. GITT profile, Open-circuit voltage curves and overpotential curves of the mesoporous $\text{LiFe}_{1-x}\text{Mn}_x\text{PO}_4/\text{C}$ cell during charge and discharge.

to an increase of the polarization. After a full oxidation of Fe^{2+} to Fe^{3+} , the reaction shifts to the two phase Mn^{2+} oxidation regime. Then, lithium ions in the surface area of particle but associated by local $\text{Mn}^{2+}-\text{O}$ units are extracted out. Due to a shortening of the diffusion length compared to the end of the first reaction regime, the polarization decrease suddenly, then increases again due to the increase of the diffusion near the end of the Mn^{2+} oxidation reaction regime. The discharging (lithium insertion) occurs at the opposite processes.

All the three samples showed the overpotential values of the $\text{Mn}^{2+}/\text{Mn}^{3+}$ redox couple (80 mV) are close to that of the $\text{Fe}^{2+}/\text{Fe}^{3+}$ couple (60 mV) (Fig. 8). The low overpotential values in both $\text{Mn}^{2+}/\text{Mn}^{3+}$ redox couple and $\text{Fe}^{2+}/\text{Fe}^{3+}$ redox couple indicates that the kinetic property of $\text{Mn}^{2+}/\text{Mn}^{3+}$ redox couple is much enhanced. From the comparison of the overpotential values of $\text{LiFe}_{1-x}\text{Mn}_x\text{PO}_4$ ($x=0.7, 0.8, 0.9$)/C with that of LiFePO_4/C , it is clearly seen that

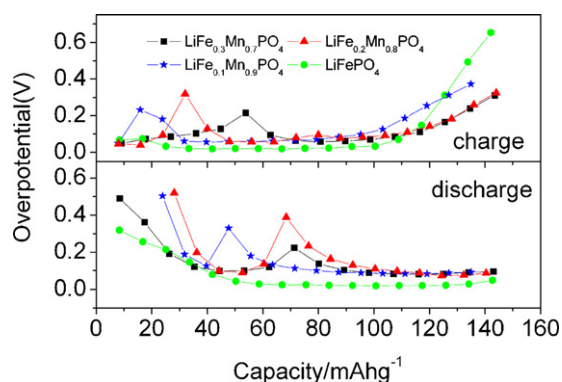


Fig. 8. Comparison of overpotential among various compositions of the $\text{LiFe}_{1-x}\text{Mn}_x\text{PO}_4/\text{C}$.

LiFePO_4 showed a much lower overpotential and no overpotential maximum appears. In consideration of the higher ionic and electronic conductivity for LiFePO_4 than LiMnPO_4 , it is reasonable that the overpotentials mainly come from charge transport.

From all the $\text{LiFe}_{1-x}\text{Mn}_x\text{PO}_4/\text{C}$ ($x=0.7, 0.8, 0.9$) we could see that the discharge capacity in the 4 V region is obviously lower than that of the charge capacity, while the discharge capacity is slightly larger than the charge capacity in the 3.5 V region. This may come from the overpotential dependence of the activation energy for phase transformation [33]. This irreversible and asymmetric phenomenon is reproducible in the GITT experimental although the galvanostatic test did not show this difference.

4. Conclusion

These mesoporous Mn rich $\text{LiFe}_{1-x}\text{Mn}_x\text{PO}_4$ ($x=0.7, 0.8, 0.9$) materials show enhanced electrochemical performances. According to the voltage hysteresis and overpotential variation of the GITT curves, Li ion diffusion in the solid solution is supposed to be the rate determining step for Li extraction and intercalation. Overpotential corresponding to the $\text{Mn}^{2+}/\text{Mn}^{3+}$ redox couple is comparable to that of $\text{Fe}^{2+}/\text{Fe}^{3+}$ redox couple in the lattice, the existence of $\text{Fe}^{2+}/\text{Fe}^{3+}$ contributes to the enhancement of the kinetic property of the $\text{Mn}^{2+}/\text{Mn}^{3+}$ redox couple.

Acknowledgement

The work in CAS was supported by "973" project (2007CB936501) and Nature Scientific Foundation of China (50730005).

References

- [1] A. Padhi, J.B. Goodenough, *J. Electrochem. Soc.* 144 (1997) 1188–1194.
- [2] A. Padhi, K.S. Nanjunclawamy, C. Masquelier, S. Okada, J.B. Goodenough, *J. Electrochem. Soc.* 144 (1997) 1609–1613.
- [3] C. Delacourt, L. Laffont, R. Bouchet, C. Wurm, J.B. Leriche, M. Morcette, J.M. Tarascon, C. Masquelier, *J. Electrochem. Soc.* 152 (2005) A913–A921.
- [4] M. Yonemura, A. Yamada, Y. Takei, N. Sonoyama, R. Kanno, *J. Electrochem. Soc.* 151 (2004) A1352–A1356.
- [5] J. Molenda, W. Ojczyk, K. swierczek, W. Zajac, F. Krok, J. Dygas, R.S. Liu, *Solid State Ionics* 177 (2006) 2617–2624.
- [6] P.P. Prosin, M. Lisi, D. Zane, M. Pasquali, *Solid State Ionics* 148 (2002) 45–51.
- [7] S.Y. Chung, J.T. Blocking, Y.M. Chiang, *Nat. Mater.* 1 (2002) 123–128.
- [8] A. Yamada, S.C. Chung, K. Hinokuma, *J. Electrochem. Soc.* 148 (2001) A224–A229.
- [9] S.F. Yang, P.Y. Zavalij, M.S. Whittingham, *Electrochem. Commun.* 3 (2001) 505–508.
- [10] S.F. Yang, Y.N. Song, P.Y. Zavalij, M.S. Whittingham, *Electrochem. Commun.* 4 (2002) 239–244.
- [11] C. Delacourt, P. Poizot, S. Levasseur, C. Masquelier, *Electrochem. Solid State Lett.* 9 (2006) A352–A355.
- [12] Z. Bakenov, I. Taniguchi, *Electrochem. Commun.* 12 (2010) 75–78.
- [13] N. Ravet, J.B. Goodenough, S. Besner, M. Simoneau, P. Hovington, M. Armand, *Electrochem. Soc. Meet. Abstr.* 196 (1999), N 127.
- [14] H. Huang, S.C. Yin, L.F. Nazar, *Electrochem. Solid State Lett.* 4 (2001) A170–A172.
- [15] Z. Chen, J.R. Dahn, *J. Electrochem. Soc.* 149 (2002) A1184–A1189.
- [16] R. Dominko, M. Bele, M. Gaberscek, M. Remskar, D. Hanzel, J. Jamnik, *J. Electrochem. Soc.* 152 (2005) A858–A863.
- [17] G.H. Li, H. Azuma, M. Tohda, *Electrochem. Solid State Lett.* 5 (2002) A135–A137.
- [18] M. Gaberscek, R. Dominko, M. Bele, M. Remskar, D. Hanzel, J. Jamnik, *Solid State Ionics* 176 (2005) 1801–1805.
- [19] A. Yamada, Y. Kudo, K.Y. Liu, *J. Electrochem. Soc.* 148 (2001) A747–A754.
- [20] A. Yamada, S.C. Chung, *J. Electrochem. Soc.* 148 (2001) A960–A967.
- [21] G.H. Li, H. Azuma, M. Tohda, *J. Electrochem. Soc.* 149 (2002) A743–A747.
- [22] X.J. Wang, X.Y. Yu, H. Li, X.Q. Yang, J. McBreen, X.J. Huang, *Electrochem. Commun.* 10 (2008) 1347–1350.
- [23] H. Gwon, D.H. Seo, S.W. Kim, J. Kim, K. Kang, *Adv. Funct. Mater.* 19 (2009) 3285–3292.
- [24] Y.U. Park, J. Kim, H. Gwon, D.H. Seo, S.W. Kim, K. Kang, *Chem. Mater.* 22 (2010) 2573–2581.
- [25] A. Yamada, Y. Kudo, K.Y. Liu, *J. Electrochem. Soc.* 148 (2001) A1153–A1158.
- [26] P.G. Bruce, B. Scrosati, J.M. Tarason, *Angew. Chem. Int. Ed.* 47 (2008) 2930–2946.
- [27] S.K. Martha, J. Grinblat, O. Haik, E. Zinigrad, T. Drezen, J.H. Miners, I. Exnar, A. Kay, B. Markovsky, D. Aurbach, *Adv. Funct. Mater.* 48 (2009) 9559–9563.
- [28] B. Zhang, X.J. Wang, Z.J. Liu, H. Li, X.J. Huang, *J. Electrochem. Soc.* 157 (2010) A283–A287.
- [29] W. Wepper, R.A. Huggins, *J. Electrochem. Soc.* 124 (1977) 1569–1578.
- [30] A.L. Patterson, *Phys. Rev.* 56 (1939) 978–982.
- [31] W. Dreyer, J. Jamnik, C. Guhlke, R. Huth, J. Moskon, M. Gaberscek, *Nat. Mater.* 9 (2010) 448–453.
- [32] G. Kobayashi, A. Yamada, R. Kanno, Y. Ohno, *J. Power Sources* 189 (2009) 397–401.
- [33] M. Tang, H.Y. Huang, N. Meethong, Y.H. Kao, W.C. Carter, Y.M. Chiang, *Chem. Mater.* 21 (2009) 1557–1571.